Available online at www.sciencedirect.com
SCIENCE DIRECT®
Polymer 44 (2003) 6663–6674
polymer
www.elsevier.com/locate/polymer

Grazing incidence X-ray diffraction studies on the structures of polyurethane films and their effects on adhesion to Al substrates

Jangsoon Kim[a,*,1], Earle Ryba[a], Jianming Bai[b]

[a]*Department of Materials Science and Engineering, The Pennsylvania State University, University Park, PA 16802, USA*
[b]*High Temperature Materials Laboratory, Oak Ridge National Laboratory, 1 Bethel Valley Road, TN 37831-6062, USA*

Received 2 May 2003; received in revised form 19 July 2003; accepted 25 July 2003

Abstract

Grazing incidence X-ray diffraction was carried out to analyze the structure of polyurethane films as a function of X-ray penetration depth by varying the angle of incidence. Coherence lengths, interplanar spacings, and crystallinities were obtained for non-aged and aged films of OH numbers of 120, 375, and 600 bonded to an aluminum substrate. Aging led to the improvement of bulk crystallinity of all the samples, particularly in the case of the aged PU-375 film, for which a dramatic increase of the bond strength was observed. The crystallinity of non-aged samples varied from the air/polymer surface down to the polymer/aluminum interface. Invariance of coherence length from air surface to interface was observed for PU-120 and PU-375 samples, implying that substrate-induced ordering has little effect on the average crystallite size. As the X-ray penetration increases near the polymer/Al interface, interplanar spacing of (021) reflection in all the films approach the value found for a bulk polyurethane-urea by Ishihara et al. The bond strength of the polyurethane film to the aluminum was exponentially proportional to the crystallinity including the crystalline interphase formed near the substrate. It is also found that the polymer film containing more (100) planes provided higher bond strength.
© 2003 Elsevier Ltd. All rights reserved.

Keywords: Polyurethane; Crystallization; Adhesion

1. Introduction

When a semi-crystalline polymer solidifies on a solid surface, its surface-induced morphology is typically spherulitic in character. The spherulites are formed by heterogeneous nucleation at a plethora of nucleation sites, such as defects and contaminants on the substrate surface. Since the substrate-induced crystallites constitute the interfacial area between the two materials, their characteristics affect adhesion of the polymer to the substrate.

Many studies have demonstrated that the crystallinity in a polymer bulk and/or at the interface dominates bond strength [1–11]. Yokoya et al. [12] showed the importance of polymer bulk crystallinity in poly(ethylene terephthalate); the polymer crystals appear to behave as physical crosslinkers below T_m, and, consequently, limit the molecular chain mobility at the interface. These polymer bulk crystals reduce adhesion due to insufficient wetting of substrate surface by the polymer chains. The molecules are mobile above the melting point, giving rise to better wetting and greater adhesion. Kestenbach et al. [13] showed that adhesion is best at interfaces where epitaxial crystallization of polyethylene on a rubber surface was observed. However, their studies used imaging techniques, which do not reveal the essential characteristics of the buried crystalline region close to the substrate surface, expected to be the most crucial for adhesion. According to Frisch et al. [14], a polyester-based polyurethane adhesive sometimes does not adhere to a substrate surface, but, instead, forms 'islands' due to the crystallization of the polyurethane. Sanchez-Adsuar et al. [15] reported that increased crystallinity in the polymer bulk increases the cohesion of polyurethane and affects the locus of failure of the bond. However, the correlation of specific crystallographic characteristics with adhesion in polymer/metal bond systems has not been clearly established. Even though the properties of the polymer, modified near the metal surface, were found to be

* Corresponding author. Tel.: +1-82-42-866-2528; fax: +1-82-42-862-6069.
E-mail address: jangskim@lgchem.com (J. Kim).
[1] Present Address: Corporate R&D, LG Chem, Ltd./Research Park, 104-1, Moonji-dong, Yuseong-gu, Daejeon, 305-380, South Korea.

0032-3861/$ - see front matter © 2003 Elsevier Ltd. All rights reserved.
doi:10.1016/S0032-3861(03)00682-7

extremely important to adhesion, these studies dealt with the crystallization in the polymer bulk rather than at the interface. Chatterjee et al. [16] suggested that a substrate surface may have active sites such as cracks or fissures inside which crystalline residues can survive at temperatures sufficient to melt the polymer on the rest of the substrate, owing to the increase in bonding of the polymer to the substrate at these sites. As the only explanation of the effect of interfacial crystallization on adhesion, this suggestion accounts for many of the facts related to heterogeneous nucleation. However, the relation of the structural aspects of the crystallites, formed at the interfacial area, to adhesion has never been reported, presumably due to the difficulty in characterizing the buried crystalline interphase.

It is true that adhesion of polymer film to substrate depends on both the cohesion of polymer and the interfacial features between polymer and substrate. The bulk properties of the polymer that corresponds to the cohesion of polymer are considered as the terms of crystallinity and crosslink density, whereas the interfacial features are determined by roughness, surface energy, and other specific morphology. For the previous publication of Ref. [17], the adhesion of polyurethane films to Al substrate was determined by the interfacial properties rather than cohesion of polyurethane films. Therefore, experimental technique to be able to characterize the interfacial features was needed to understand how this interfacial property, especially crystallites formed at interfacial area, contributes to the adhesion of polyurethane films to Al substrate. Hence, this study concerns the correlation of adhesion of polyurethane to an Al substrate with specific crystallographic characteristics of the polyurethane crystalline interphase induced by the Al substrate. Although the morphological features at the interface have been investigated [17], it is difficult to characterize the structure of the crystallites by means of conventional imaging techniques. Grazing incidence angle X-ray diffraction (GIXD) was employed here to characterize certain features of the crystalline portion of the polymer. In particular, the crystallinity of the polyurethane films, the coherence length of the ordered molecular regions, the specific orientation of substrate-induced crystallites, and the extent of molecular ordering were determined. Since polymers consist of low atomic number elements, with small atomic scattering factors, and only small amounts of crystalline material are present, a synchrotron source was used. GIXD scans reveal the buried polyurethane crystalline interphase formed on the Al surface. The diffraction results were correlated with bond strengths from Kim and Ryba [17].

2. Experimental

The polyether polyols used in this study were provided by Arch Chemicals, Inc. The polyol OH numbers were 120 (oxypropylated and ethylated glycerol), 375 (propoxylated glycerol), and 600 (aliphatic amine based polyol), corresponding to polyol molecular weights of 1400, 596 and 374, respectively. In order to form the urethane linkage, these polyols were reacted with diphenylmethane-4:4′-diisocyanate (MDI) (Aldrich) in the solvent dimethylformamide (DMF). The synthesis of three polyurethane solutions, PU-120, PU-375 and PU-600, with an isocyanate index of 105, was performed at 50 °C with stirring for 1 min. For the measurement of the effect of crystallization on bond strength, 3% solutions were cast on approximately 1000 Å thick Al films, sputtered on Si wafers held at 50 °C. For these samples, solvent was evaporated at room temperature in air for 72 h and subsequently in vacuum for one week. Aging was done for 28 h at 170 °C, followed by air-cooling. The thicknesses of the polyurethane films, measured by an optical microscope, are listed in Table 1. N indicates non-aged, and A aged polyurethane film.

GIXD measurements were performed on beamline X14A at the National Synchrotron Light Source (NSLS, Brookhaven National Laboratory). A diagram of the experimental setup is shown in Fig. 1. A cylindrical mirror with variable curvature was used to focus the vertical divergence of the beam at the specimen position. The monochromator consists of a water-cooled flat first crystal and a conically bent focusing second crystal. An X-ray energy of 8.048 keV ($\lambda = 1.54076$ Å) was used. A 0.5 mm × 0.5 mm incident beam slit was used to limit the beam to the specimen surface at small incident angles. The scattering measurements were conducted using a Huber four-circle diffractometer with the sample nearly vertical. Due to the low scattering power and small scattering volume, a 0.5 mm × 4.0 mm (horizontal) receiving slit was used.

The instrument resolution depended on the X-ray experimental set-up, since the analyzer crystal was not used. Thus, the instrumental broadening for a $\theta - 2\theta$ scan was determined by the detector slit size and the distance from the sample to the slit, and was 0.05°.

Scattering measurements were carried out using a symmetric four-circle diffraction geometry in which the angles of the incident and diffracted beams with respect to the substrate surface, α_i and α_f (see Fig. 2), are equal.

Table 1
Thickness of polyurethane films

	Thickness (μm)
NPU-120	19 ± 7
APU-120	13 ± 3
NPU-375	15 ± 3
APU-375	13 ± 3
NPU-600	13 ± 3
APU-600	14 ± 3

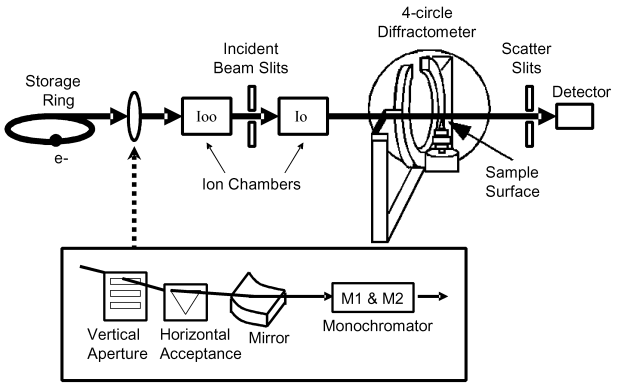

Fig. 1. Diagram of the beamline X14A geometry. The beam is focused using the variable curvature cylindrical mirror, and the energy is chosen by setting the first and second crystal monochromators.

2.1. Grazing Incident Angle X-ray Diffraction (GIXD)

X-rays incident at below the critical angle α_c are subject to total external reflection (Fig. 3) [18]. However, by increasing the angle of incidence above the critical angle, one can probe layers of increasing thickness and explore various crystallographic features in successively greater portions of a film from the air/film interface to the film/substrate interface [19–26].

Radiation of wavelength λ incident at an angle α_i to a film surface is both reflected and refracted (Fig. 3). The refractive index [27], n, of the film is generally expressed as

$$n = 1 - \delta - i\beta \tag{1}$$

with

$$\delta = \frac{\lambda^2 N r_e Z}{2\pi} = \frac{\lambda^2}{2\pi}\left(\frac{b}{V}\right) \tag{2}$$

$$\beta = \frac{\lambda N \sigma_a}{4\pi} = \frac{\lambda \mu}{4\pi} \tag{3}$$

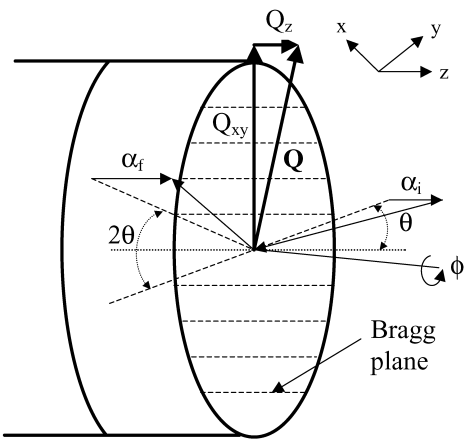

Fig. 2. Scattering geometry for grazing angle incidence diffraction. For the GIXD mode, i.e. $0 < \alpha_f < 3 \sim 5°$, $2\theta \gg \alpha_i$ and α_f, so that $Q = (Q_{xy}; Q_z)$, where $Q_{xy} \approx 4\pi \sin\theta/\lambda \gg Q_z \sim 2\pi \sin\alpha_f/\lambda$. The sample is $\theta - 2\theta$ scanned, and Q_{xy} is measured in the direction of the sample surface. To investigate the polymer/substrate interface, the angle of incidence α_i is varied.

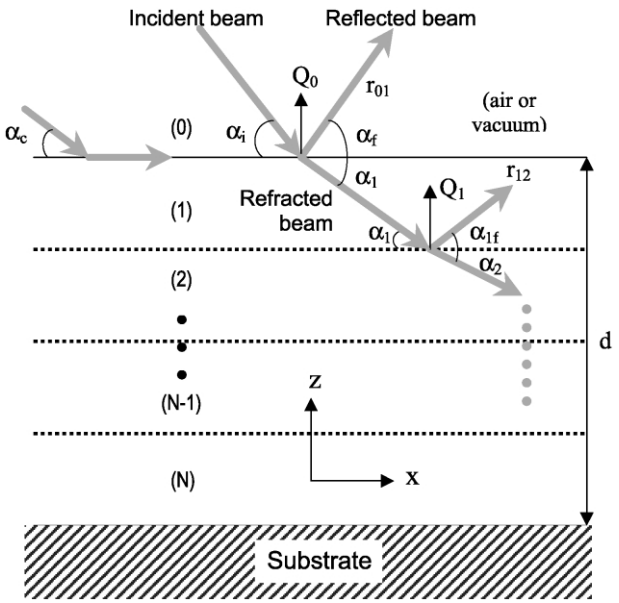

Fig. 3. The reflected and transmitted waves for a layer with two interfaces [18]. The wave-vectors in vacuum (Q_0) and in the layer (Q_1) are shown. Scattering angles and reflection coefficients r are also indicated. The total film thickness is d. At the critical angle, total external reflection of X-ray beam occurs.

$$\sigma_a = 1.6726A\frac{\mu}{\rho} \tag{4}$$

where the classical electron radius $r_e = 2.814 \times 10^{-5}$ Å, N is Avogadro's number, Z is the atomic number, ρ (g/cm^3) the density of the film, A the atomic mass, and σ_a the absorption cross section, defined as the number of photons absorbed per second by an atom divided by the flux of the incident radiation. λ (Å) $= 12.1/E$ (keV), (b/V) the scattering length density, and the linear absorption coefficient μ denotes the probability of a photon being absorbed while traversing the material to the depth of a unit length. Here, the scattering length b represents the strength of the interaction of the radiation and the elementary scatterer. For most polymers, δ is of the order of 10^{-6} for both X-rays and neutrons. The extinction coefficient β for Cu K_α X-rays is about 10^{-2} to 10^{-3} times δ for most materials.

At an interface separating two media with refractive indices n_0 and n_1, the ratio of the refractive indices will determine the angle at which radiation is refracted, α_1, in comparison with the angle of incidence, α_0, of the radiation on the interface. Snell's law [27] is

$$n_0 \cos\alpha_i = n_1 \cos\alpha_1 \tag{5}$$

If the interface of concern is one between air and a solid, then $n_0 = 1$, and

$$\cos\alpha_1 = \cos\alpha_0/n_1 \tag{6}$$

For X-rays, $\delta > 1$, then $n_1 < 1$, so there is a real angle of refraction for all angles of incidence, provided that α_0 is greater than the critical angle α_c. The angle of refraction, α_1,

is zero at:

$$\cos \alpha_c = \cos \alpha_0 = n_1 \quad (7)$$

In the event that α_1 is zero, the refracted ray runs parallel to the film surface and does not penetrate into the film. This condition defines the critical angle, α_c ($= \alpha_i$ in the above equation when $\alpha_1 = 0°$), below which total external reflection occurs. The X-ray critical angle, to within a very good approximation, is [27]:

$$\alpha_c = (2\delta)^{1/2} = \lambda\left[\frac{Nr_eZ}{\pi}\right]^{1/2} = 2.317\lambda\sqrt{\frac{\rho Z}{A}} \quad (8)$$

where α_c is on the order of milliradians. The critical angles, measured by specular scans in the 2θ range of $0.1 \sim 2°$, for the polyurethane films used in this work are listed in Table 2. Aging the films changed the polyurethane surface component because of migration of polymer chain soft segments toward the polyurethane surface, and, thus, resulted in changes in the critical angles.

The angle of incidence α_i is of the order of a few tenth of degrees; this angle determines the irradiation depth. The penetration depth Λ [27] is given by

$$\Lambda = \left(\frac{\lambda}{\sqrt{2}\pi}\right)\{[(\alpha_i^2 - \alpha_c^2)^2 + (2\beta)^2]^{1/2} - (\alpha_i^2 - \alpha_c^2)\}^{-1/2} \quad (9)$$

where the extinction coefficient β arises due to the adsorption of X-rays by material. The variation of the penetration depth for these polyurethanes, non-aged and aged, and aluminum as a function of the angle of incidence α_i is shown in Fig. 4. The angle of incidence was determined to order to characterize the material from the polymer surface down to the polymer/Al interface.

The peak position, peak half width, and integrated intensity were determined for each diffraction maximum. From the peak position, the spacing d of the diffracting planes was calculated:

$$d = 2\pi/Q = \lambda/2 \sin \theta_B \quad (10)$$

where Q is the wave vector, $4\pi \sin \theta/\lambda$. The peak width at half maximum, B, is inversely proportional to the average correlation length (CL), i.e. the dimension of a crystal domain [30]:

$$CL = \frac{0.9\lambda}{B\cos\theta_B} \quad (11)$$

Table 2
Critical angles for polyurethane films. N indicates non-aged, and A aged

	Critical angle (degree)
Aluminum	0.232
NPU-120	0.186
APU-120	0.205
NPU-375	0.190
APU-375	0.283
NPU-600	0.203
APU-600	0.304

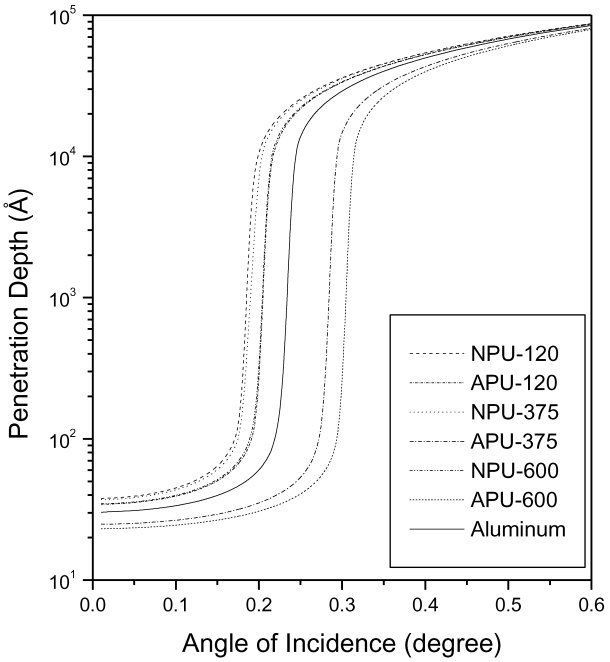

Fig. 4. X-ray penetration depths for the polyurethane sample and the aluminum substrate at 8.048 keV ($\lambda = 1.540755$ Å). The penetration depth varies exponentially below the critical angle. Above the critical angle, the penetration is limited only by absorption.

The scattering data were curve-fitted in the following manner. The 2θ scan range was $10 \sim 30°$; all of the intense crystalline peaks were found in this range. In order to isolate the scattering data from the polymer film only, the scan from a bare Al substrate was used to remove the background. After subtracting the background and the Bragg peaks for Al, the scattering from the polymer films only was obtained. Subsequently, the peaks in the scattering curve were profile fitted. Fitting with a Gaussian function gave a lower χ^2 value than for a Lorentzian function, and did not represent the data well. The best fit was determined by the goodness of the fit (i.e. comparison of the χ^2 values). The peaks were indexed using the diffraction data for a polyurethane-urea, listed in Table 3, given by Ishihara et al. [31] for monoclinic unit cell with dimensions $a = 4.72$, $b = 11.33$, c (chain axis) $= 11.64$ Å, and $\gamma = 116.5°$ (Fig. 5). The Bragg peak

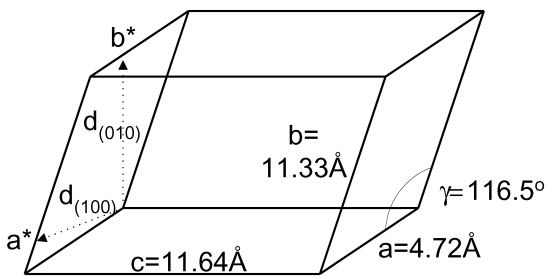

Fig. 5. Monoclinic unit cell of polyurethane-urea suggested by Ishihara et al. [31], assuming two molecular chains per unit cell. The c-direction corresponds to the chain axis. The b-axis corresponds to the stacking of polymer main-chains on top of each other. The reciprocal a^* and b^*-axes are normal to the bc-plane and the ac-plane, respectively.

Table 3
Powder pattern for polyurethane-urea observed by Ishihara et al. [31]. The pattern was recorded using a Rigaku Denki RU-3 X-ray equipment with a 5 cm radius and a flat plate camera with Ni-filtered Cu K_α radiation ($\lambda = 1.5418$ Å). v-very, s-strong, m-medium, and w-weak

hkl	2θ	*d* (Å)	Relative intensity
020	17.48	5.07	m
021	19.07	4.65	s
100	21.04	4.22	vs
$1\bar{1}2$	24.30	3.66	m
111	27.34	3.26	m
103	31.25	2.86	w
040	35.46	2.53	w
041	36.20	2.48	vvw
$1\bar{1}4$	36.20	2.48	vvw
122	36.66	2.45	vw
$2\bar{2}0$	38.11	2.36	w
$1\bar{3}4$	40.23	2.24	w
$2\bar{4}0$	41.59	2.17	vw
200	42.83	2.11	vw
202	45.55	1.99	vw
211	48.38	1.88	vvw
140	49.50	1.84	w
$3\bar{2}0$	59.61	1.55	vw

positions and intensities from wide angle X-ray diffraction scans from both non-aged and aged samples are in satisfactory agreement with those for the peaks found by Ishihara et al. [31] (see Table 4). Furthermore, the hard segment of this polymer consists of only MDI and terminated urethane-urea functional groups. FTIR spectra for all the polyurethane films showed the existence of urea groups which were probably formed from the reaction of MDI with water molecules in the air. Thus, the use of the powder pattern of Ishihara et al. is appropriate.

The fitted results were used to calculate crystallinities (total area under crystalline peaks/(total area under crystalline + amorphous peaks)), interplanar spacings (Eq. (10)), and coherence lengths (CL) (Eq. (11)). The instrumental broadening on beamline X14A was very small (0.05° 2θ), and was neglected in the calculation of the coherence lengths from the very broad Bragg reflections from the polymer for all the samples. The crystallinity, coherence length (CL), and interplanar spacing *d* were then plotted as a function of X-ray penetration depth (Λ).

Table 4
Comparison of powder pattern observed by Ishihara et al. [31] and wide-angle X-ray diffraction on six polyurethanes used in this study. The *I* indicates a percent intensity ratio under intensity of 100 at a (100) reflection

Ishihara et al. [31]	(*hkl*)	(111)	(100)	(021)	(020)
	d	3.26	4.22	4.65	5.07
	I	m	vs	s	m
NPU-120	*d*	3.334	4.216	4.740	–
	I	23.6	100	34.3	–
APU-120	*d*	3.312	4.210	4.636	5.060
	I	15.8	100	65.0	21.2
NPU-375	*d*	3.353	4.201	4.697	5.004
	I	17.2	100	56.7	51.1
APU-375	*d*	3.304	4.202	4.666	5.002
	I	13.5	100	54.3	21.9
NPU-600	*d*	3.334	4.207	4.688	5.001
	I	28.4	100	38.0	29.8
APU-600	*d*	3.315	4.202	4.690	5.005
	I	18.7	100	41.3	28.2

3. Results and discussion

The solution cast polyurethanes crystallize on the Al surface at grain boundaries, defects, and impurities [17]. This is called 'substrate-induced crystallization'; spherulites are nucleated and grow. Depending on the molecular weight and functionality of the polyol, and the heat treatment, the number density and size of the spherulites varied. Fig. 6 shows GIXD scans for the non-aged and aged PU-120, PU-375, and PU-600 films. Five or six angles of incidence were used to examine the change of crystallinity along the film depth. The polymer peaks were indexed according to the powder pattern given by Ishihara et al. [31] for the crystal structure of polyurethane-urea.

The (020) reflection was not obvious in the scan for the non-aged PU-120 sample, whereas the scan of the aged PU-120 film exhibited a definite (020) peak. This suggests that aging causes reorganization of polymer chains such that the hard segments in the PU-120 sample gather in the stacking direction corresponding to the [020], aligned by van der Waals force between benzene rings. In addition, aging led to an increase in crystallinity in the bulk portion of the films, as shown in Fig. 7, resulting from chain rearrangements due to the high mobility of the component molecules at the aging temperature. Heat treatment is also important with respect to the packing efficiency of the polymer chains; it is likely that additional chain strands get into periodic registry upon aging. These effects of aging were particularly notable for the PU-375 sample; additional reflections ((020) and (111)) appear, and (100) and (021) reflections were sharper than for the aged PU-120 and PU-600 samples. From diffraction scans at varying angles of incidence, it can be seen that the enhanced ordering of the polymer molecules was likely induced by the interaction of the substrate and polymer.

The peak profiles were curve-fitted, and the individual peak profiles were used to calculate a measure of crystallinity from the ratio of the total area under the crystalline peaks and the total area over the angular range of the data. As shown in Fig. 7, the crystallinity in the non-aged samples increased with angle of incidence up to 0.883°, beyond which it remained constant. At an angle of incidence of 0.883°, where the X-ray penetration depth is about 13 μm, the scattering originates from the film/substrate interface in addition to the bulk film. Substrate-induced crystallization was definitely observed in the non-aged samples since the crystallinity increased near the interface. All the aged samples exhibited essentially constant crystallinity through the entire film, due to crystal thickening and an increase in

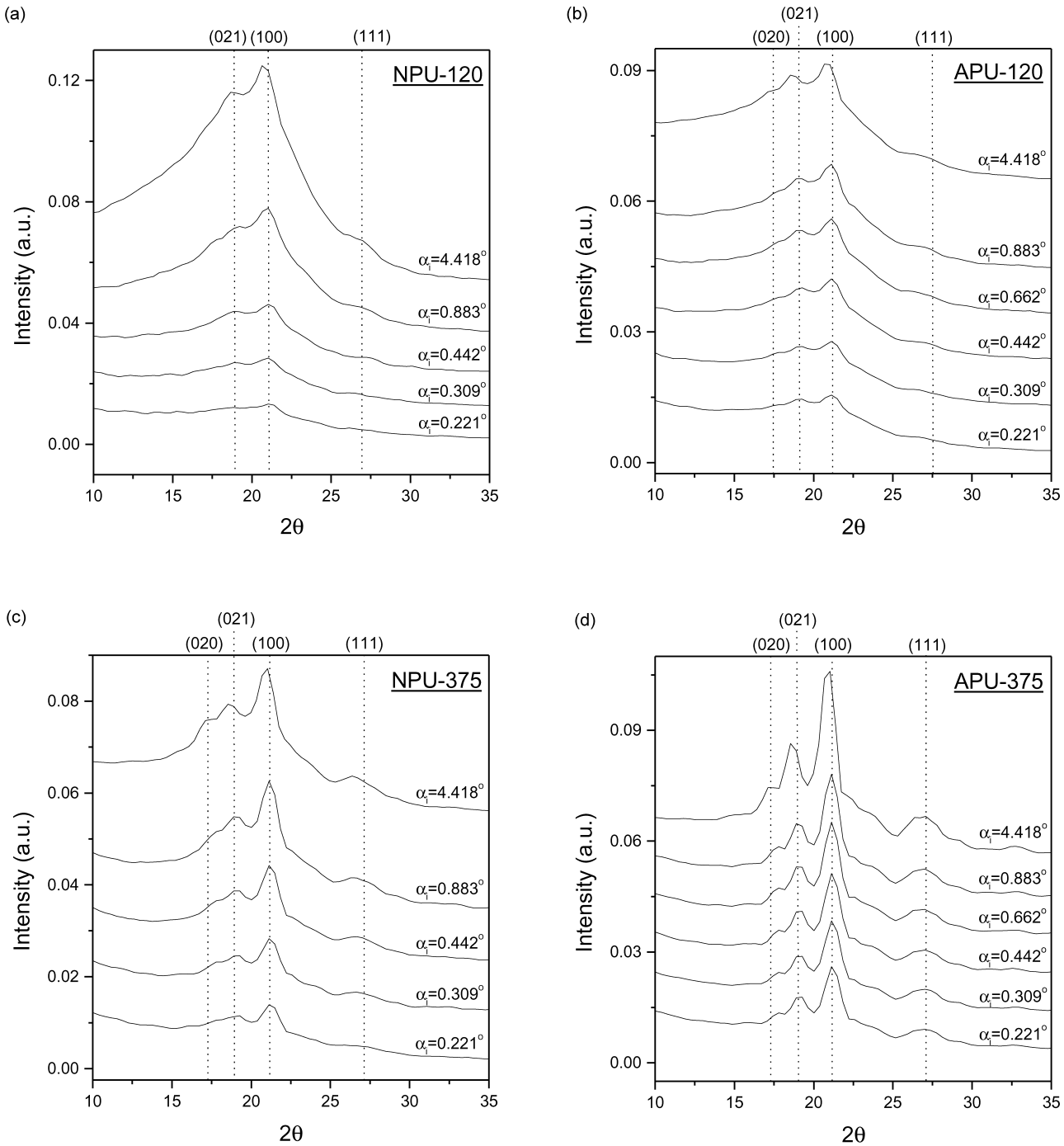

Fig. 6. GIXD scans, background and Al peak subtracted to isolate the scattering data from the polymer film only, for the polyurethane films at various angles of incidence. The peaks indicated by the dotted lines are considered crystalline peaks.

the perfection of the existing crystallites within the bulk film during the curing process. Overall, the aged PU-120 and PU-600 samples exhibited an increase in crystallinity in the bulk film, while aging led to the increase of crystallinity in both the bulk and interface regions for the PU-375 film. Such a variation in the crystallinity was confirmed by optical micrographs with an example of the PU-375 films in Fig. 8. The polyurethane spherulites in the APU-375 film were present from the air polymer surface down to the Al interface, resulting in the constant crystallinity through the entire film. Most of the spherulites in the NPU-375 film existed near the polymer/Al interface. Thus, it is evident that the substrate-induced crystallization occurred in the non-aged sample. The PU-120 and PU-600 samples also exhibited the similar distribution of the polymer spherulites (not shown). This optical investigation corresponds to the

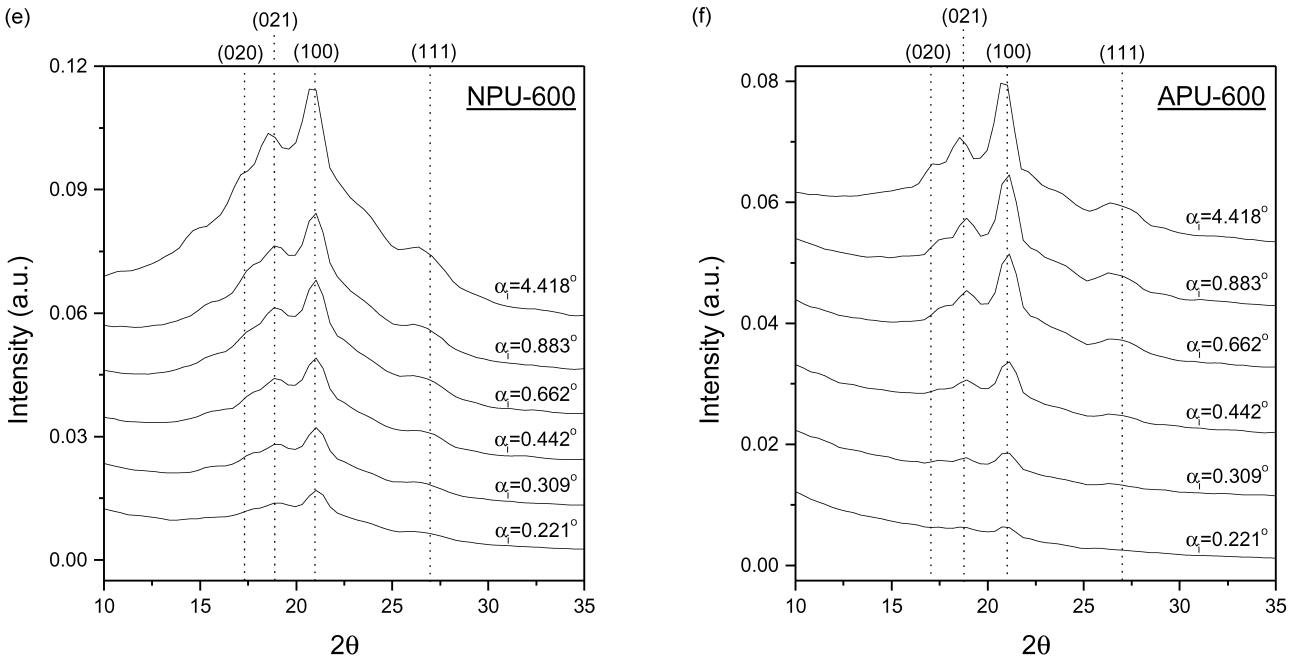

Fig. 6 (*continued*)

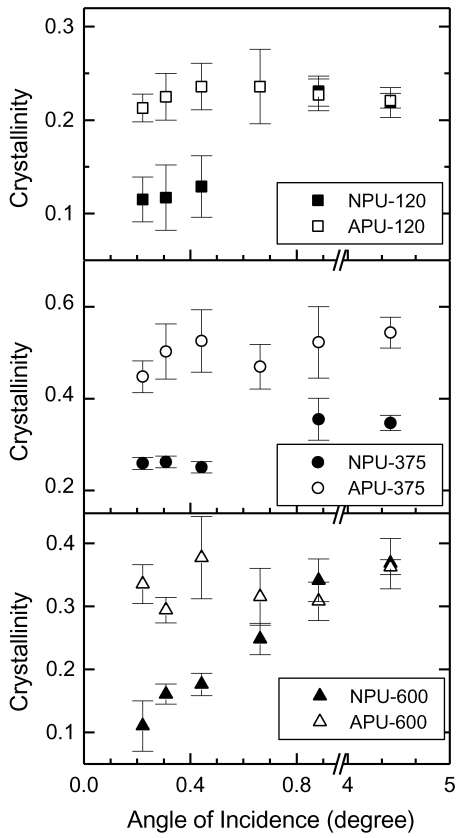

Fig. 7. Variation in crystallinity along film depth from the air surface to the polymer/Al interface. The crystallinity is constant beyond an angle of incidence of 0.883°, where the scan includes scattering from the crystalline interphase. The penetration depth at this angle coincides with the measured film thickness.

variation in crystallinity along film depth, obtained from the grazing incidence X-ray diffraction.

There is a trade-off between crosslink density and phase separation. In general, phase mixing occurs if the molecular weight of the polyol is below 1000. The PU-120 sample, with a polyol molecular mass of 1400, has a greater possibility of phase separation of the soft and hard segments. The PU-600 sample should have the highest crosslink density due to its smaller polyol molecular weight and higher functionality. Bhatia et al. [28] and Hearn et al. [29] have reported that the soft segments in polyurethane migrate to near the air surface, while the hard segments aggregate closer to the interface at the substrate surface and form crystal domains. For the PU-120 sample, the hard segments have to migrate along with the higher molecular weight soft segments. The highly crosslinked network in the PU-600 sample must be broken in order for the hard segments to diffuse towards the interface. The PU-375 sample has a lower crosslink density than the PU-600 sample and less phase separation than the PU-120 sample. Thus, in the PU-375 sample, hard segments likely migrate relatively easily to the film/substrate interface where they align to form crystal domains, resulting in higher crystallinity near the interface. Crystallization of the aged samples probably takes place at various heterogeneities inside the bulk polymer at the aging temperature. Therefore, the crystallinities of the aged films are expected to be constant throughout.

The extent of molecular ordering is often evaluated by measuring the width of Bragg reflections. The full width of a peak at half maximum (FWHM) is converted to a coherence length (CL). The coherence length provides an estimate of

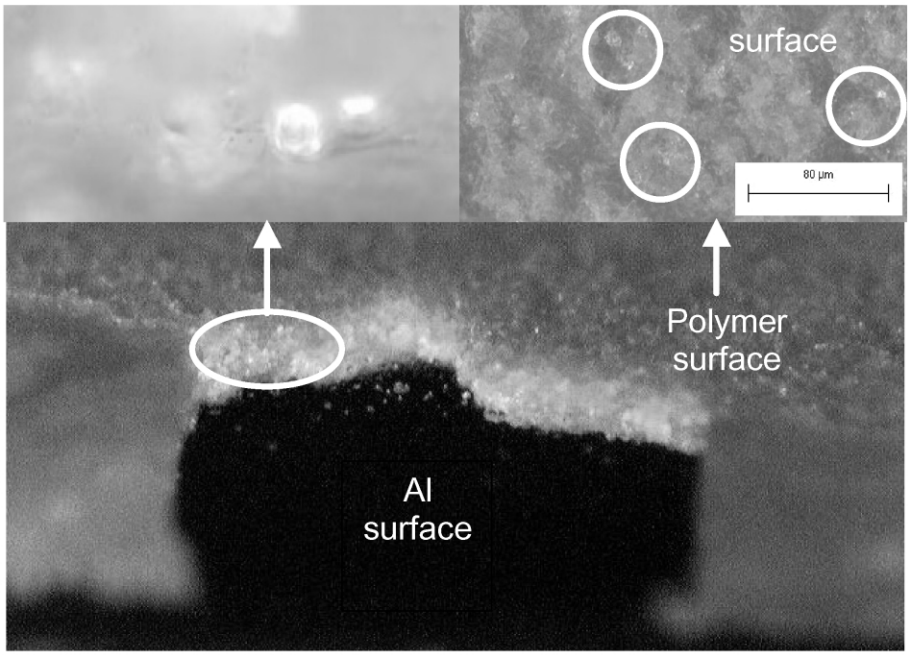

(a)

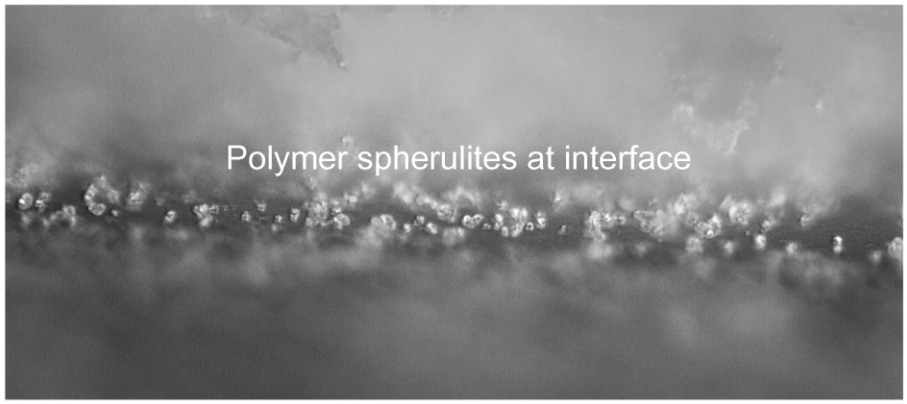

(b)

Fig. 8. Optical micrographs of the APU-375 (a) and NPU-375 (b) films under crossed polars; specimen tilted 30° except for the APU-375 film surface image (upper right in image (a)). Spherulites are present through entire film in the aged sample, while the spherulites appeared near the polymer/Al interface in the non-aged sample.

the average size of the scattering domains. Using Eq. (11), coherence lengths were calculated, assuming no contribution of microstrain to the peak broadening. These are shown as a function of penetration depth in Fig. 9. Although the range of the coherence lengths observed differed in each sample, an overall invariance from the air surface to the film/substrate interface was found. This does not mean that chain alignment was not enhanced near the Al surface. $CL_{(100)}$, defined as the average size of the scattering domains in a direction perpendicular to the (100) planes, ranged from 70 to 95 Å for all samples. Aging of the PU-375 samples resulted in a notable increase in $CL_{(021)}$, the average size of the scattering domains in a direction perpendicular to the (021) planes. The data for the PU-120 and PU-600 films suggest that there is a similar, but smaller thickening of the scattering domains in the same direction. This increased coherence length on aging is a result of secondary crystallization; the crystallites became larger in the direction of the stacking of the polymer chains on top of each other along the *b*-axis, defined in Fig. 5. Aging appears to extend polymer chain ordering over greater distances. The mechanism for increasing order along the stacking direction is not obvious, but the following, assuming that crystallization of the polyurethane starts at the Al surface and any heterogeneities in the bulk polymer which are active at the aging temperature. The first polymer strands immobilized from the solution adhere to the substrate surface. When the surface is completely covered by chain

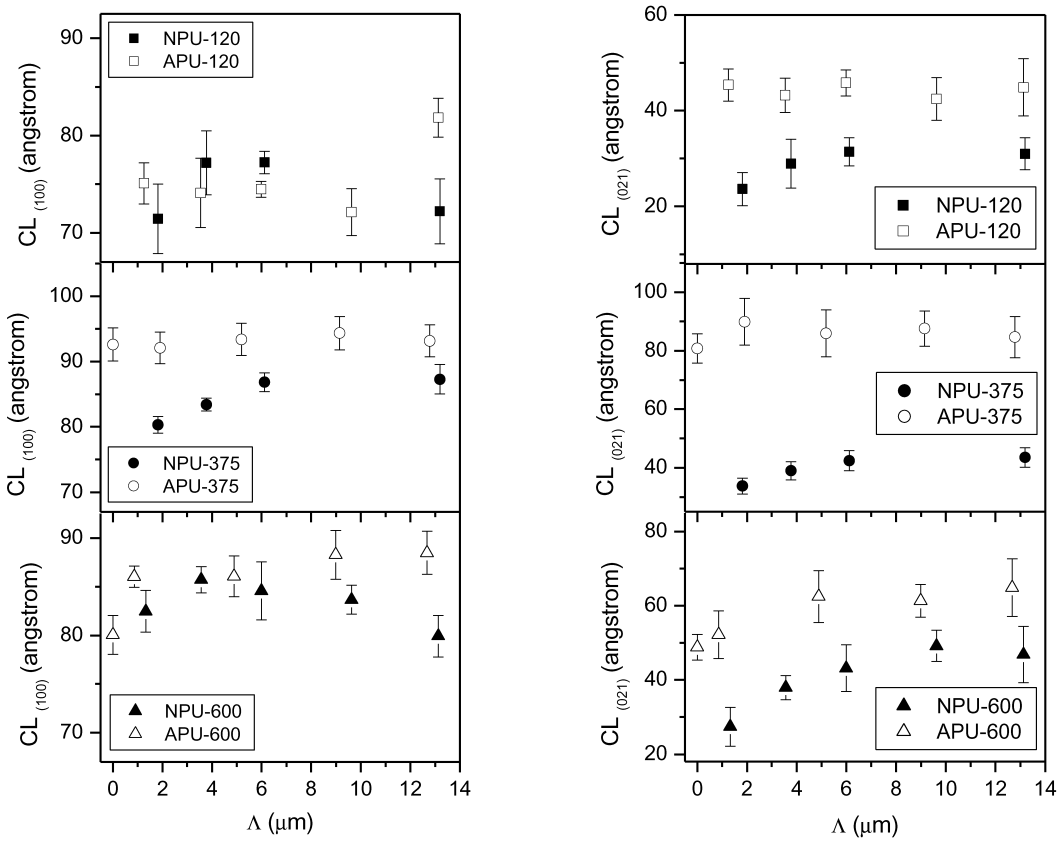

Fig. 9. Variation in coherence length as a function of X-ray penetration depth. Aging does not lead to the increase of $CL_{(100)}$ for PU-120 and PU-600 films. In contrast, aging resulted in an increase of $CL_{(021)}$ for all the samples.

segments, further alignment of new chain segments takes place at the ends of the folds of previously aligned chains. These chains may not select the same folding and orientation as those of the ones on which they nucleate. As this process continues, the chains will orient differently, resulting in randomly distributed orientations. The GIXD scans indicate that crystallization in the non-aged sample occurred mainly at the polymer/Al interface, and in the aged samples, at both the Al surface and the heterogeneities inside the bulk polymer.

From the GIXD scans, a change in d with penetration depth was observed for each reflection (Fig. 10). These reflections can be attributed to an interchain packing or density correlation between neighboring chains. The (020) peak in the GIXD was not clear to obtain the exact Bragg angle position, while this reflection in the wide angle X-ray diffraction was obvious to be able to compare intensities with the patterns observed by Ishihara et al. [31]. The fitting result for the (020) reflection was used only for calculation of crystallinity. The appearance of the unclear (020) peak in the GIXD implies such that X-ray beam is parallel to the (020) planes. It turns out that the polyurethane hard segments align in parallel against the Al surface. Instead, the $d_{(021)}$ is analyzed to understand how polymer molecules arrange in the stacking direction. The $d_{(021)}$s for all the samples before and after aging were significantly different. Apparently, the stacking of polymer chains on top of each other from layer to layer is influenced by the presence of the substrate. A negligible change in $d_{(100)}$, the interchain spacing, was also seen in all the samples. This results from the fact that the interaction between chains was not affected by the presence of the Al surface. As the GIXD scans contain scattering from the crystalline interphase, the interplanar spacings for (021) reflection for all the aged samples approach, overall, the value ($d_{(021)} = 4.65$ Å) found for a bulk polyurethane-urea by Ishihara et al. It indicates that Al surface-induced order in the stacking direction follows the order of a bulk polyurethane-urea in Table 3, and vanishes away from the interface.

Since the GIXD scans at an angle of incidence of 0.883°, where the X-ray penetration depth is around 13 μm, included scattering from all material down to the film/substrate interface, the crystallographic characteristics obtained at this depth contain information from the polyurethane crystalline interphase formed on Al surface. The findings were related to bond strength measured by indentation debonding [17]. Fig. 11 shows that the bond strength of the polyurethane/Al samples increased with the crystallinity, as measured at the angle of incidence of 0.883°. Higher crystallinity for the whole film apparently results in stronger

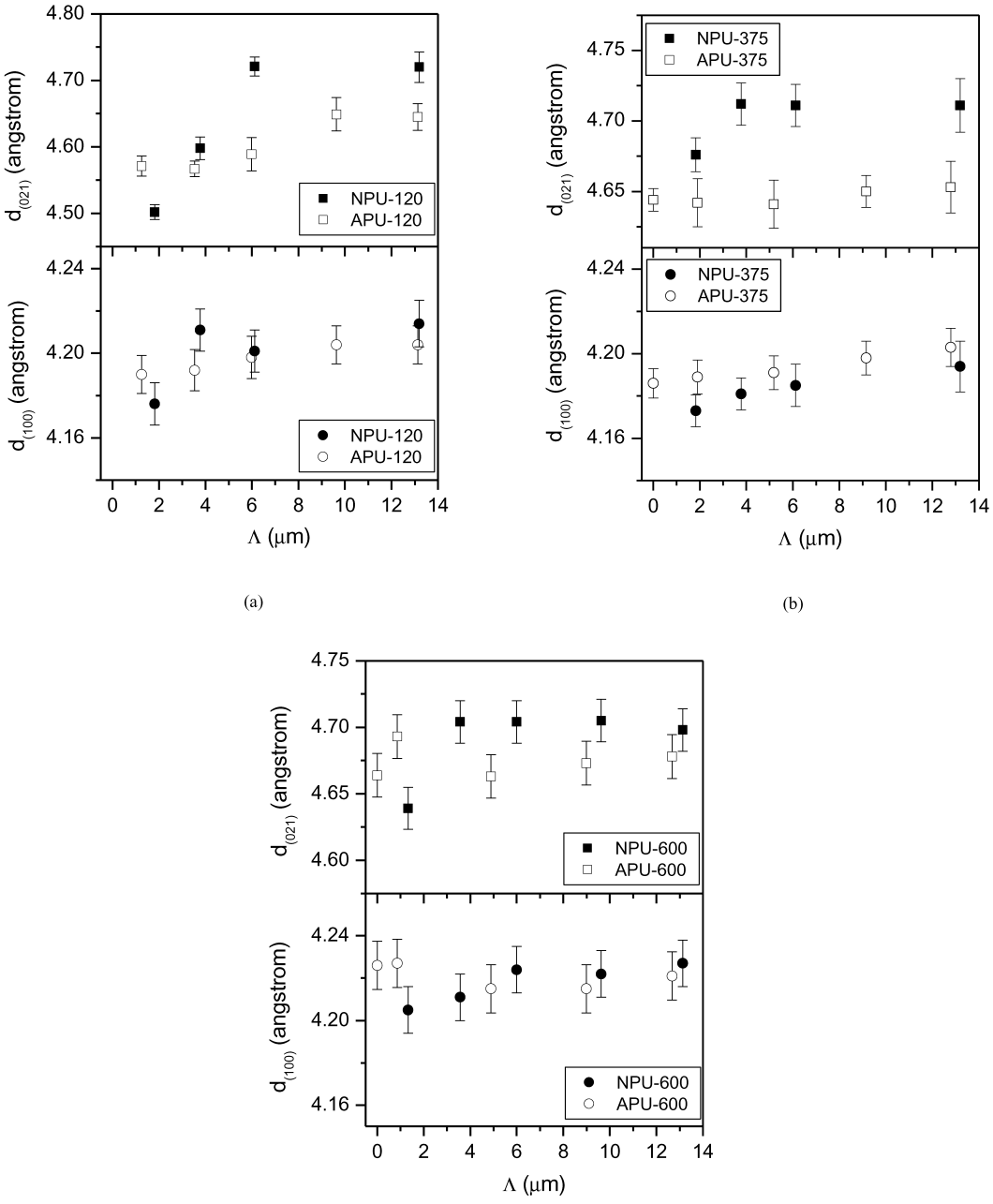

Fig. 10. Variation in $d_{(021)}$ and $d_{(100)}$ as a function of penetration depth in (a) PU-120, (b) PU-375, and (c) PU-600 films. For the (021) reflections in the non-aged samples, the d varies significantly from the air surface to the interface.

bonding between the two materials. The following discusses the relation of adhesion to the crystallinity of the polymer film, including the interphase formed on Al substrate. Chatterjee et al. [16] suggested that heterogeneities, such as insoluble foreign impurities, take the form of particles that contain crevices capable of being wetted by the molten polymer. On cooling, the polymer crystallizes in the crevices, but a higher temperature than the bulk melting point is required to melt the crystals in the cracks because of adhesion of the polymer to the particles. The higher melting phase may induce the crystallization of the lower melting material, following a particular orientation relationship that could increase the number and/or the strength of the bonds that form across the interface. The crystalline regions physically crosslink with the amorphous phase and should inhibit the soft segments from preferentially migrating to the air surface. As the bulk crystallinity of the material increases, the concentration of physical crosslinks increases, thus making it configurationally harder for soft segments to locate near the air surface. If higher crystallinity is attained

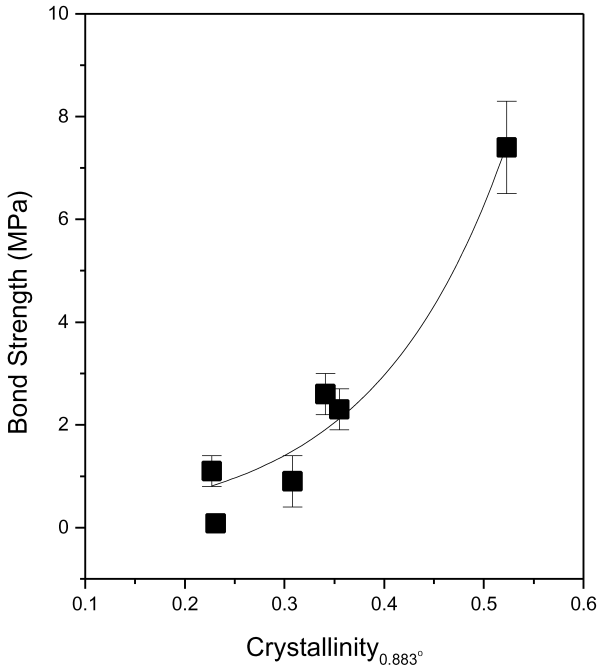

Fig. 11. The relation of bond strength to crystallinity obtained from scattering data at an angle of incidence of 0.883°, at which the penetration depth coincides with the film thickness.

through the entire film, it provides higher bond strength due to increase of polymer bulk strength, as shown in the aged PU-375 sample, in that the interfacial adhesion, from *mechanical deformation bonding theory* [32], is determined by the mechanical strength of the polymer bulk film. In fact, the adhesion of polymer film to substrate depends on both cohesion of polymer and interfacial properties between polymer and substrate. The equation [17] used to calculate the bond strength in this study was established by considering both cohesion of polymer film and interfacial features between polymer and substrate; the equation consists of elastic modulus, Poisson's ratio, debonding ratio, film thickness etc. The elastic modulus is determined by the cohesion of polymer, whereas the interfacial properties are considered as a term of debonding ratio. The elastic modulus of the polymer increases with the bulk crystallinity of the polymer film. This does not, subsequently, guarantee the improvement of the bond strength, since the adhesion should be determined by both bulk and interfacial properties of polymer film. From the previous publication of Ref. [17], the bond strength in the current materials system was related to the morphological features at interface between polyurethane film and Al substrate, and, further, aging affected variation of the bond strength. However, it was not found that there was a clear relation of adhesion to the crystallization of the polyurethane film. From Fig. 11, it is evident that higher bulk crystallinity improves the cohesion of polyurethane films, resulting in the increase of bond strength of polyurethane to Al substrate. However, even though the increase of bond strength measured in this study has included the considerable contribution of the cohesion of polymer, the interfacial features in terms of the interfacial crystallization at the interface between two materials should still be considered. This is explained in terms of chain alignment in the following.

The more interesting question is whether the chain alignment inside the polymer crystallites near the Al surface is associated with bond strength. In Fig. 12, the relationship of the bond strength to the ratio of the (021) and (100) integrated intensities, obtained at the angle of incidence of 0.883°, is shown. The ordering along [021] inversely affects the bond strength. That is, greater molecular order along the *a*-axis (see Fig. 5) led to a higher bond strength. The molecular ordering over the relatively short distance between the (100) planes is accomplished by hydrogen bonding between hard segments, but the ordering of polymer molecules over the larger distance between the (021) planes by weak van der Waals bonds. Thus, it is harder to separate the polymer film containing more (100) planes than (021) planes. Subsequently, the bond strength increased, as the integrated intensity of (100) plane over (021) plane becomes greater.

4. Conclusions

From GIXD scans for different depths of penetration, substrate-induced ordering was found to be significant in non-aged samples, while aging led to the improvement of crystallinity throughout all of the polyurethane films. The variation of the crystallinity in non-aged and aged samples

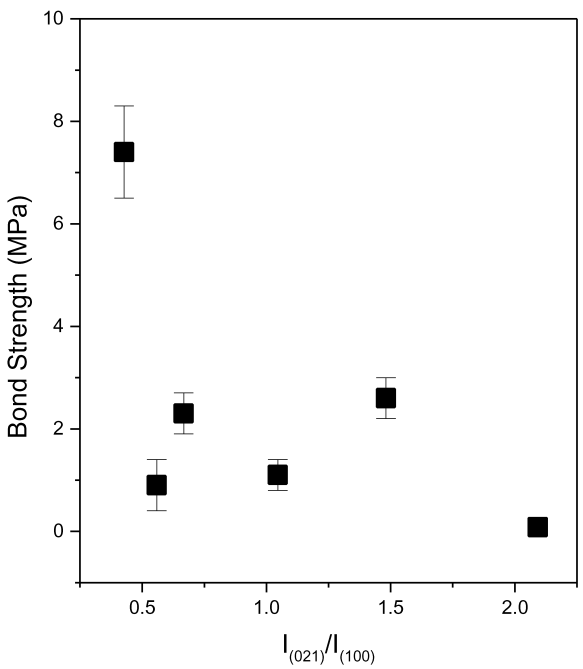

Fig. 12. The relation of bond strength to the ratio of the integrated intensities of the (100) and (021) reflections, obtained at an angle of incidence of 0.883°.

corresponded to the optical micrographs showing the distribution of the spherulites from the air polymer surface down to the polymer/Al interface. An invariance of $CL_{(021)}$ and $CL_{(100)}$ from air surface to interface was observed in the PU-120 and PU-375 samples, implying that substrate-induced ordering did not affect the average crystallite size. The crystallinity measured from the scattering including the polyurethane crystalline interphase, was exponentially proportional to bond strength. It was also found that the bulk crystallinity in polyurethane contributed considerably to adhesion. The bond strength was improved with the integrated intensity of (100) plane over (021) plane, due to the stronger hydrogen bonding force between polyurethane hard segments than van der Waals force between the stacking directions of the polymer segments, respectively. As a consequence, the increase of the adhesion with the bulk crystallinity was resulted from the improvement of cohesion of polyurethane film as well as the contribution of interfacial feature such as difference in polymer chain alignment.

Acknowledgements

This work was supported by Air Products and Chemicals Inc. This research was performed in part at beamline X14A of the National Synchrotron Light Source, Upton, NY. X14A is operated by the High Temperature Materials Laboratory User Program of Oak Ridge National Laboratory, which is sponsored by the Assistant Secretary for Energy Efficiency and Renewable Energy, office of Transportation Technology under contract No. DE-AC05-00OR22725. The NSLS synchrotron facility is sponsored by the Office of Science, US Department of Energy under grant no. DE-AC02-76CH00016.

References

[1] Yegorenkon NI. Polym Sci USSR 1980;22:94.
[2] Tuinstra F, Koenig JL. J Comp Mater 1970;4:492.
[3] Cheng FS, Kardos JL, Tolbert TL. SPE J 1970;26:62.
[4] Bessell T, Shortall JB. J Mater Sci 1975;10:2035.
[5] Kantz MR, Corneliussen RD. Polym Lett 1973;11:279.
[6] Fitchmus DR, Newman S, Wiggle R. J Appl Polym Sci 1970;14:2441.
[7] Fitchmus DR, Newman S, Wiggle R. J Appl Polym Sci 1970;14:2457.
[8] Schonhorn H, Ryan FW. J Adhesion 1969;1:43.
[9] Schonhorn H, Ryan FW. J Polym Sci A-2 1968;6:231.
[10] Nakao K. J Adhesion 1972;4:95.
[11] Love BJ. Heat and mass transfer in solidification processing. ASME 1991;175:121.
[12] Yokoya H, Porter RS. J Appl Polym Sci 1972;44:1679.
[13] Kestenbach HJ, Loos J, Petermann J. Polym Engng Sci 1998;38:478.
[14] Frisch KC, Xiao HX, Czerwinski RW. Adhesives Age 1988;41.
[15] Sanchez-Adsuar MS, Martin-Martinez JM. J Adhesion Sci Technol 1997;11:1077.
[16] Chatterjee AM, Price FP, Newman S. J Polym Sci 1975;13:2391.
[17] Kim J, Ryba E. J Adhesion Sci Technol 2001;15:1747.
[18] Slawecki TM. An experimental investigation of surface segregation and phase separation in thin binary polymer blend films, PhD Thesis, The Pennsylvania State University; 1995.
[19] Takahashi T, Inamura M, Tsujimoto I. Polym Lett 1970;8:651.
[20] Tuinstra F, Baer E. Polym Lett 1970;8:861.
[21] Campbell D, Qayyum MM. J Polym Sci Polym Phys 1980;18:83.
[22] Rickert SE, Baer E, Wittmann JC, Kovacs AJ. J Polym Sci Polym Phys 1978;16:895.
[23] Wang C, Liu CR. Polymer 1999;40:289.
[24] Thomason JL, Vanrooyen AA. J Mater Sci 1972;27:889.
[25] Thomason JL, Vanrooyen AA. J Mater Sci 1972;27:897.
[26] Burton RH, Day TM, Folkes MJ. Polym Commun 1984;25:361.
[27] Tolan M. X-ray scattering from soft-matter thin films. Berlin: Springer; 1999.
[28] Bhatia QS, Burrell MC. Polymer 1991;32:1948.
[29] Hearn MJ, Ratner BD, Briggs D. Macromolecules 1988;21:2950.
[30] Cullity BD. Elements of X-ray diffraction, 2nd ed. London: Addison-Wesley; 1978.
[31] Ishihara H, Kimura I, Yoshihara N. J Macromol Sci Phys 1983;B22:713.
[32] Boiziau C, Lecayon G. Surf Inter Anal 1988;12:475.